The Astrophysical Journal, 705:L143–L147, 2009 November 10 doi:10.1088/0004-637X/705/2/L143

PLASMA HEATING IN THE VERY EARLY PHASE OF SOLAR FLARES

M. Siarkowski[1], R. Falewicz[2], and P. Rudawy[2]
[1] Space Research Centre, Polish Academy of Sciences, 51-622 Wrocław, ul. Kopernika 11, Poland; ms@cbk.pan.wroc.pl
[2] Astronomical Institute, University of Wrocław, 51-622 Wrocław, ul. Kopernika 11, Poland; falewicz@astro.uni.wroc.pl, rudawy@astro.uni.wroc.pl
Received 2009 June 22; accepted 2009 October 2; published 2009 October 21

ABSTRACT

In this Letter, we analyze soft X-ray (SXR) and hard X-ray (HXR) emission of the 2002 September 20 M1.8 *GOES* class solar flare observed by the *RHESSI* and *GOES* satellites. In this flare event, SXR emission precedes the onset of the main bulk HXR emission by ∼5 minutes. This suggests that an additional heating mechanism may be at work at the early beginning of the flare. However, *RHESSI* spectra indicate a presence of the non-thermal electrons also before the impulsive phase. So, we assumed that a dominant energy transport mechanism during the rise phase of solar flares is electron-beam-driven evaporation. We used non-thermal electron beams derived from *RHESSI* spectra as the heating source in a hydrodynamic model of the analyzed flare. We showed that energy delivered by non-thermal electron beams is sufficient to heat the flare loop to temperatures in which it emits SXR closely following the *GOES* 1–8 Å light curve. We also analyze the number of non-thermal electrons, the low-energy cutoff, electron spectral indices, and the changes of these parameters with time.

Key words: Sun: flares – Sun: X-rays, gamma rays

1. INTRODUCTION

It is commonly accepted that during the impulsive phase of the solar flare, non-thermal electron beams accelerated anywhere in the solar corona move along magnetic field lines to the chromosphere where they deposit their energy. Here, most non-thermal electrons lose their energy in Coulomb collisions while a small fraction ($\sim 10^{-5}$) of the electrons' energy is converted into hard X-rays (HXRs) by the bremsstrahlung process. The heated chromospheric plasma evaporates and radiates over a wide spectral range from HXRs or gamma rays to radio emission. All processes described above, commonly called the electron beam-driven evaporation model, are believed to be the dominant energy transport mechanisms during solar flares. One of the most spectacular and well-observed manifestation of the described processes is soft X-ray (SXR) emission of magnetic loops observed, e.g., by the *Yohkoh* and *Hinode* satellites. Such a scenario implies that the HXR and SXR fluxes emitted by solar flares are generally related, as was first described by Neupert (1968). Since HXR and microwave emissions are produced by non-thermal electrons and SXRs are the thermal emission of a hot plasma, the Neupert effect confirms that non-thermal electrons deliver energy spent on plasma heating. Thus, the HXR emission is directly related to the flux of the accelerated electrons whereas the SXR emission is related to the energy deposited by the non-thermal electron flux.

This interpretation, however, leads to a number of problems and questions concerning energy content and time relations between SXR and HXR fluxes (see, e.g., Dennis 1988; Dennis & Zarro 1993; McTierman et al. 1999).

There are several papers that investigate temporal dependencies between the beginnings of SXR and HXR emissions. For example, Machado et al. (1986) and Schmal et al. (1989) reported frequent strong SXR emission before the impulsive phase. Following these authors, on average, the SXR emission precedes the onset of HXR emission by about 2 minutes. Veronig et al. (2002) analyzed 503 solar flares observed simultaneously in HXR, SXR, and Hα. In more than 90% of the analyzed flares, an increase of SXR emission began prior to the impulsive phase. On average, the SXR emission starts 3 minutes before the HXR emission.

An enhanced thermal emission preceding the onset of the HXRs may be indicative of a thermal preheating phase prior to the impulsive electron acceleration. Current-sheet models (e.g., Heyvaerts 1977) of solar flares predict a preheating phase. Li et al. (1987) discussed the preheating phase of solar flares triggered by new emerging magnetic flux. They proposed four different types of reconnections to explain the preheating as well as impulsive phases of flares.

Another approach to this issue is multi-thread hydrodynamic modeling of solar flares. Warren (2006) suggested that modeling a flare as a bunch of independently heated threads may simulate precedence of the SXR emission. The author successfully reproduced the temporal evolution of high-temperature flare plasma in the Masuda flare of 1992 January 13.

An alternative mechanism to electron beam-driven evaporation, namely, conducted-driven evaporation, was developed recently by Battaglia et al. (2009). They studied in detail the pre-flare phase of four solar flares using imaging and spectroscopy from the *RHESSI* satellite. These authors explain the time evolution of the observed emission for all analyzed events as an effect of saturated heat flux.

The tendency of the SXR flux to appear before HXRs emission can be attributed also to the sensitivity threshold of the HXR detectors (Dennis 1988). At the beginning of the flare, the energy flux may be below the detection threshold of HXR emission.

In this Letter we show, using unprecedented high sensitivity of the *RHESSI* detectors (Lin et al. 2002) and a numerical model of flare, that early SXR emission observed prior to the impulsive phase could be fully explained without any ad hoc assumptions (at least for analyzed event). All necessary energy to explain the soft emission could be derived from observed HXR spectra. In Section 2, we describe the analyzed event. Section 3 presents the details of the HXR spectra fitting, numerical modeling, and the results. The discussion and conclusions are presented in Section 4.

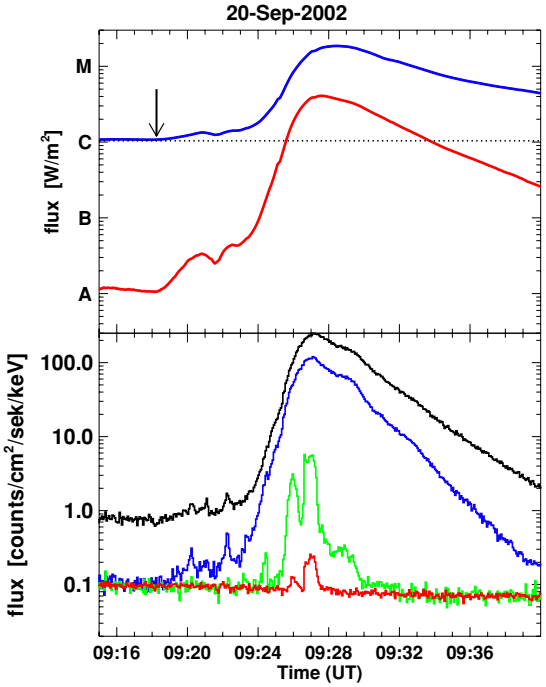

Figure 1. Top panel: *GOES* light curves in two energy bands: 1–8 Å (upper line) and 0.5–4 Å. The horizontal dotted line represents the preflare background level observed in soft channel. The arrow indicates the starting moment of the numerical model. Bottom panel: *RHESSI* light curves taken in four energy bands (from top to bottom): 4–12, 12–25, 25–50, and 100–300 keV.

2. OBSERVATIONS

For our work, we selected *RHESSI* observations obtained without the activation of the attenuators in order to prevent discontinuities in fitting parameters. A solar flare with a simple single-loop structure was then chosen for convenience in numerical modeling. The investigated flare occurred in the southwest hemisphere in active region (AR) NOAA 10126 (S23E69) on 2002 September 20. It was classified as an M1.8 *GOES* class flare. *GOES* X-ray light curves of the flare are shown in Figure 1 (top panel). *GOES* (1–8 Å) flux has a background level of 1.04×10^{-6} W m^{-2} (C1.04). The SXR emission started to increase slowly at 09:18:15 UT and showed two local maxima at 09:21:00 UT and 09:22:30 UT. It reached its maximum at 09:28:30 UT. Harder (0.5–4 Å) *GOES* emission started to increase at the same time as the softer one and peaked 1 minute earlier at 09:27:30 UT. It also showed two local, even more pronounced maxima of the emission.

RHESSI X-ray light curves of the flare taken in four energy bands are shown in Figure 1 (bottom panel). The impulsive phase in X-rays $\gtrsim$25 keV started at 09:25:24 UT and it had two maxima around 09:26 UT and 09:27 UT, respectively. In 25–50 keV energy range, a small spike of emission occurred between 09:24:16 UT and 09:24:32 UT. It appeared also as a small hump on the both *GOES* light curves. The X-ray emission below 25 keV started to rise simultaneously with *GOES* emission. Three local peaks of emission are presented in these energy bands at the moments of SXR local maxima.

Images obtained using *RHESSI* data with the CLEAN imaging algorithm revealed SXR emission at 6–12 keV and intermediate energy emission 12–25 keV coincident with the flare location. These observations indicate that SXR emission recorded by *GOES* in the early phase of flare came from analyzed event.

Images obtained with the PIXON imaging algorithm (Hurford et al. 2002) showed a single flare loop (see Figure 2). This

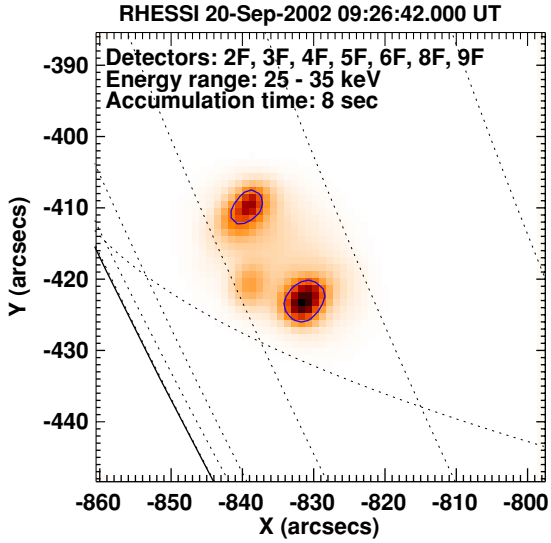

Figure 2. 25–35 keV PIXON image with time accumulation from 09:26:42 UT to 09:26:50 UT, at maximum impulsive phase. An isocontour corresponds to 30% of the maximum flux.

image allows us to define geometrical proportions of the loop. The cross sections of the loop $S = 1.13 \times 10^{17}$ cm^2 was estimated as an area within a level equal to 30% of the maximum flux in the 25–35 keV energy range. Half-length of the loop $L_0 = 9.5 \times 10^8$ cm^2 was estimated from the distances between the centers of gravity of the footpoints, assuming a semi-circular loop shape.

Unfortunately, *SOHO*/EIT telescope observed this AR before an after the flare. However, images obtained with 195 Å filter after event at 09:47:59 and 9:59:59 UT confirmed the single-loop structure of the flare.

3. CALCULATIONS/MODELING OF THE HEATING OF THE LOOP

The *RHESSI* data were analyzed using *RHESSI* OSPEX package of the SolarSoftWare (SSW) system. Data were summed over the front segments of the seven detectors with detectors number 2 and 7 excluded. The spectra were measured with 4 s temporal resolution in 158 energy bands from 4 to 300 keV. We applied the energy widths $dE = 0.3$ keV within the range 4–15 keV, $dE = 1.0$ keV in the range 15–100 keV, and $dE = 5.0$ keV above 100 keV. The analyzed spectra were corrected for pulse pile-up, decimation, and albedo effects. We used full two-dimensional detector response matrix to convert input photon fluxes to count rates. Before fitting spectra, we removed the averaged non-flare background spectra. For energies below 50 keV, the background spectra were accumulated and averaged from preflare period between 09:00 and 09:06 UT. For energies above 50 keV, we used a linear interpolations between the time intervals before and after the impulsive phase.

In our model, we used spectra taken after 09:18:15 UT when the SXR emission started to increase. We used 4 s long time bins, but after background subtraction we increased the accumulation time in the period from 09:18 UT to 09:23 UT to keep the positive counts rates in most of the energy bins in the 4–20 keV range.

The spectra were fitted with single temperature thermal plus thick-target models (vth + thick). The thermal model was defined by single temperature and emission measure of the optically thin

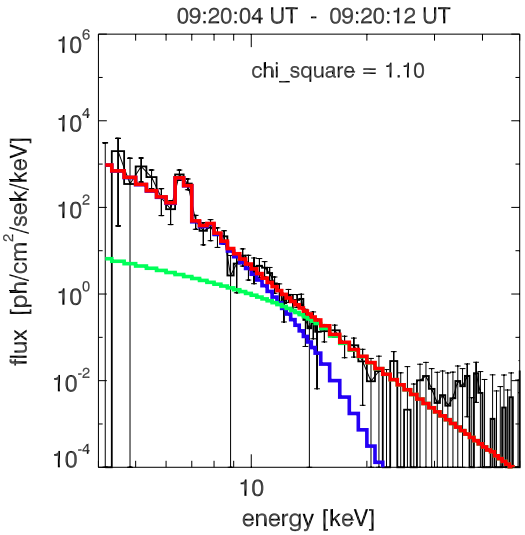

Figure 3. *RHESSI* spectral fit results for data accumulated with a 8 s time interval between 09:20:04 and 09:20:12 UT. The spectrum was fitted with one temperature thermal model (blue color) and thick-target model (green) with energy cutoff $E_c = 15.8$ keV (please see the text for more details). Total fitted spectrum is shown in red. The errors bars of the observed spectra are also shown.

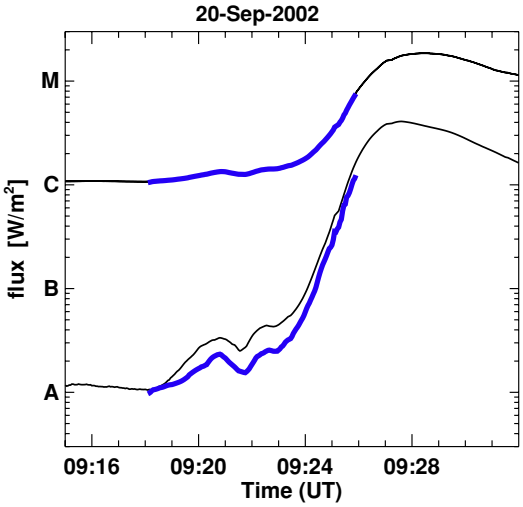

Figure 4. Comparison of the observed (black thin lines) and calculated (thick blue line) *GOES* fluxes in 1–8 Å (upper curves) and 0.5–4 Å (lower curves) energy bands during initial phase of the analyzed flare.

thermal plasma, and is based on the X-ray continuum and line emission calculated by the CHIANTI atomic code (Dere et al. 1997; Landi et al. 2006). The element abundances are based on the coronal abundances of Feldman & Laming (2000). The thick-target model was defined by the total integrated electron flux $N_{\rm nth}$, the power-law index of the electron energy distribution δ, and the low-energy cutoff of the electron distribution E_c. Figure 3 shows the fit of the spectrum, accumulated between 09:20:04 UT and 09:20:12 UT. In addition to the thermal component, there is an important power-law shape for emission between 15 keV and 20 keV which can be recognized and fitted as thick-target emission of the non-thermal electrons.

We assumed the electron beam-driven evaporation model of the solar flare. Therefore, we used in hydrodynamic model of the analyzed flare the non-thermal electrons beams derived from *RHESSI* spectra as the heating source via the Coulomb collisions. Heating was modeled using the approximation given by Fisher (1989). In this work, we used one-dimensional Naval Research Laboratory (NRL) Solar Flux Tube Model code by Mariska and his co-workers (Mariska et al. 1982, 1989). This code was slightly modified by us. We included: new radiative loss and heating functions; the VAL-C model of the initial structure of the lower part of the loop; and double precision calculations. All the changes were tested by comparison of the results with the results of the original model. For details, see the paper by Falewicz et al. (2009). An important problem which we meet during the modeling of the flares using the original NRL code was an insufficient amount of the mater located in feet of the loops. To solve this problem, we applied the VAL-C model of the solar plasma, extended down using Solar Standard Model data. It was done solely in order to obtain big enough storage of the matter. All other aspects of the NRL model of the chromosphere are unchanged (radiation is suppressed, optically thick emission is not accounted for, and no account is taken of neutrals, the net conductivity flux is negligible).

We modeled the evolution of the analyzed flare as follows: an initial, quasi-stationary preflare models of the flaring loop was built using geometrical and thermodynamic parameters estimated from *RHESSI* and *GOES* data. These initial parameters of the flaring loop were as follows: semi-length 9500 km, radius 1900 km, and pressure in feet 22 dyn cm^{-2}. Small volumetric heating was used to keep this model in the quasi-stationary state on the preflare level of activity before the start of the non-thermal heating. Then, we started to model the heating of the loop by non-thermal electrons adding a dose of energy and calculating the resulting *GOES* flux. We used thick-target parameters $N_{\rm nth}$, δ and E_c obtained from fits of consecutive *RHESSI* spectra for each time step as input into the Fisher's heating function. However, an acceptable fit can be obtained for all E_c values in the range 5–30 keV for all following spectra. Because the low-energy cutoff determines an amount of energy delivered to the loop, this non-uniqueness could be limited using an independent energetic condition, like observed 1–8 Å *GOES* flux. Indeed, for each time step we adjusted E_c values in order to achieve conformity of the observed and modeled fluxes in *GOES* 1–8 Å band. Such use of *GOES* 1–8 Å flux puts important limitation on the allowed low-energy cutoff values and reduces importantly the non-uniqueness problem.

Figure 3 shows an example of the *RHESSI* fitted spectrum where the low-energy cutoff E_c was adjusted to equalize synthesized and observed *GOES* fluxes in 1–8 Å channel. The high-energy part of this spectrum was finally fitted with the following thick-target parameters: $\delta = 7.37$, $N_{\rm nth} = 7.2 \times 10^{33}$ electrons s^{-1}, and $E_c = 15.8 \pm 0.1$ keV. This non-thermal electron beam contains total energy flux $F_{\rm nth} = 2.16 \pm 0.14 \times 10^{26}$ erg s^{-1} and heated our loop during 8 s between 09:20:04 and 09:20:12 UT. The heating increases the synthesized *GOES* class in this period from B1.93 to B2.11, which exactly corresponds to the changes of the observed (with background removed) *GOES* flux. Given errors of E_c and $F_{\rm nth}$ were derived by fitting the *GOES* 1–8 Å flux with an accuracy of 0.01 W m^{-2}. Thermal component of the spectrum was fitted with emission measure EM $= 4.25 \times 10^{46}$ cm^{-3} and temperature $T_e = 14.4$ MK. Obtained temperature is consistent with temperature obtained from *GOES* data (11.0 MK). We fitted also the spectra with the purely thermal model, but obtained temperature of 20.3 MK seems to be quite high with respect to the *GOES* one and makes us more confident in the interpretation with the presence of the non-thermal electrons well before the impulsive phase.

The final result of our modeling is presented in Figure 4. The synthesized *GOES* 1–8 Å light curve closely follows the

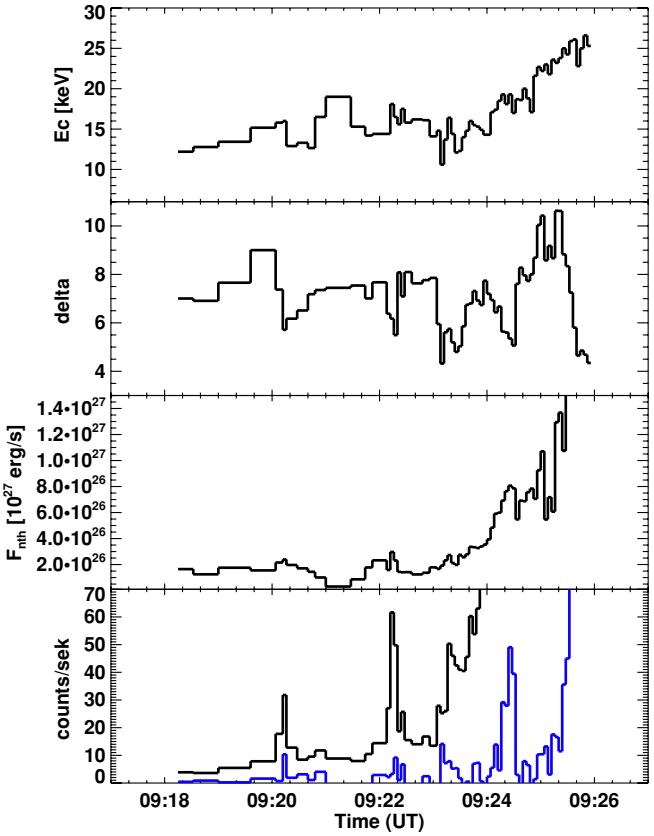

Figure 5. Time evolution of the thick-target parameters and *RHESSI* fluxes before the start of impulsive phase. From top to bottom: E_c, δ, $F_{\rm nth}$, and observed fluxes at 12–25 and 25–50 keV.

observed one. The correspondence between observed and calculated fluxes in the case of the 0.5–4 Å band is not so ideal. The inconsistency could be attributed to crude estimation of the initial loop conditions, errors in *RHESSI* spectra restoration, and the simplicity of our model. However, because the variations of the calculated 0.5–4 Å light curve did not differ too much from the observed variations, it means that our model simulates the main physical processes in right way. As a result, we fully restored the observed slow increase of the SXR flux recorded before impulsive heating using only non-thermal electrons characteristics derived from the observed HXR spectra. Thus, we confirmed that in the analyzed flare variations of the SXR and HXR fluxes are consistent with the Neupert effect.

Figure 5 presents time variations of the electron beam (*thick target*) parameters and *RHESSI* fluxes before the onset of the main bulk of HXR emission at 09:25:24 UT. Non-thermal electron distributions, characterized by these parameters, delivered to the loop an amount of energy sufficient to produce the slow increase of the *GOES* emission observed before the impulsive phase. Low-energy cutoff E_c changed during this period between 12 keV and 24 keV. Electron spectral index δ varied between 4.5 and $\simeq$10, while total electron energy flux ranges from 3.3×10^{25} erg s^{-1} to 1.4×10^{27} erg s^{-1}. Obtained variations of the E_c reflect probably temporal variations of the processes in primary energy source region. On the other side, obtained variations of the index δ show a clear general pattern of the soft–hard–soft spectral evolution (see, e.g., Grigis & Benz 2004). Additionally, all peaks in the 12–50 keV energy range are related to local increases in energy flux of the non-thermal electrons and so to local increases in heating of the loop. The two most pronounced peaks (and heating increases) at 09:20:16 UT and 09:22:16 UT were manifested as local flux enhancements on both *GOES* light curves. The maximum evaporation speed, achieved in a early phase of the simulation, was equal to 130 km s^{-1}. The maximum temperature, density, and pressure obtained at the loop apex during the modeled period were equal to 13.5 MK, 1.3×10^{11} cm^{-3}, and 462 dyn cm^{-2}, respectively.

4. CONCLUSIONS

The start and quick increase of HXR $\gtrsim$ 25 keV flux (defined as an impulsive phase of flare) is interpreted as an indication of the injection of the non-thermal electrons into the flaring loop and a beginning of the plasma heating by these electrons. However, often the SXR emission starts a few minutes earlier than the HXR which raises a question about the heating source in very early stage of the flare. Numerous solutions were proposed of which heating by thermal conduction and Multi-Stranded Loop model are the most well known. We showed that it is possible to fit SXR (*GOES*) and HXR (*RHESSI*) emissions of a solar flares well before beginning of the impulsive phase without any additional heating besides the heating by non-thermal electrons. This was made possible because of the unprecedented high sensitivity of the *RHESSI* detectors which are able to measure very low HXR flux early in the flare. Part of the emission, mainly in the energy range <25 keV, is non-thermal in nature and indicates the presence of non-thermal electrons. In this case of an M1.8 *GOES* class flare, the non-thermal electron energy fluxes of the order of 10^{26} erg s^{-1}, derived under the thick-target interpretation, fully explains the required heating of the plasma and resulting increase in SXR emission.

The main limitations of our work are crude estimation of the initial physical and geometrical parameters of the loop, errors in restoration of the *RHESSI* spectra and in *GOES* calibration, relative simplicity of the one-dimensional hydrodynamical model, and single-loop approximation of the event. While the synthesized *GOES* 1–8 Å light curve closely follows the observed one, all limitations mentioned above caused small differences between observed and calculated fluxes in the 0.5–4 Å band.

Various authors considered classical heat conduction from the loop-top energy reservoir. Battaglia et al. (2009) fitted (*RHESSI*) spectra of four flares with a purely thermal emission and claim that at least for some flares electron beam heating does not work. In a case of flare analyzed by us purely thermal spectra seems to give too high temperatures (>20 MK) comparing to those obtained from *GOES* data. Additionally, even if the HXR spectra observed with *RHESSI* provide no evidence for non-thermal particles this does not necessarily means that the electrons do not exists. As it was pointed, e.g., by Brosius & Holman (2009), the non-thermal HXR emission associated with electron beam could be below *RHESSI's* level of detection. These authors estimated that in the case of analyzed event the non-thermal X-ray emission produced by an electron beam of sufficient energy flux to heat chromospheric plasma to the temperature and emission measure observed by *RHESSI* is below the observed background level. It is possible that for some flares heat conduction and for others beam-driven evaporation works on the early phase of flare evolution. In our case, the heating of the matter caused by non-thermal electrons is 2–4 orders higher then local conductive flux. Stoiser et al. (2008) presented analytic predictions of the X-ray EM and T_e expected in single and filamented flare loops for both mechanisms of evaporation and have tested these against real data consisting

of 18 *RHESSI* microflares. Their results suggest beam heating in filamented loops to be in agreement with data. The peak temperatures were consistent with both single-loop and multi-thread heating. The observed emission measures were mostly compatible with beam driving for a number of threads, but for two events EMs were also compatible with single-loop model.

Our results extend the standard model of SXR and HXR relationship to the early phases of solar flares and thus expands the number of flares consistent with the Neupert effect. These results also indicate that the process of electrons acceleration appears during the early stage of the flare, well before the impulsive phase. This was confirmed, e.g., by Asai et al. (2006) who reported detection of the coronal non-thermal emission during the preimpulsive phase of the X4.8 flare on 2002 July 23.

Our method of adjustment of the low-energy cutoff E_c in order to equalize synthesized and observed *GOES* fluxes in 1–8 Å channel can be considered as a new method of E_c determination.

The authors acknowledge the *RHESSI* consortium. This work was supported by the Polish Ministry of Science and Higher Education, grant number N203 022 31/2991 and by the European Community's Seventh Framework Programme (FP7/2007-2013) under grant agreement no. 218816 (SOTERIA).

REFERENCES

Asai, A., Nakajima, H., Shimojo, M., White, S. M., Hudson, H. S., & Lin, R. P. 2006, PASJ, 58, L1
Battaglia, M., Fletcher, L., & Benz, A. O. 2009, A&A, 498, 891
Brosius, J. W., & Holman, G. D. 2009, ApJ, 692, 492
Dennis, B. R. 1988, Sol. Phys., 118, 49
Dennis, B. R., & Zarro, D. M. 1993, Sol. Phys., 146, 177
Dere, K. P., Landi, E., Mason, H. E., Monsignori-Fossi, B. C., & Young, P. R. 1997, A&AS, 125, 149
Falewicz, R., Rudawy, P., & Siarkowski, M. 2009, A&A, 500, 901
Feldman, U., & Laming, J. M. 2000, Phys. Scr., 61, 222
Fisher, G. H. 1989, ApJ, 346, 1019
Grigis, P. C., & Benz, A. O. 2004, A&A, 426, 1093
Heyvaerts, J., Priest, E. R., & Rust, D. M. 1977, ApJ, 216, 123
Hurford, G. J., et al. 2002, Sol. Phys., 210, 61
Landi, E., Del Zanna, G., Young, P. R., Dere, K. P., Mason, H. E., & Landini, M. 2006, ApJS, 162, 261
Li, H.-W., Pallavicini, R., & Cheng, C. 1987, Sol. Phys., 107, 271
Lin, R. P., et al. 2002, Sol. Phys., 210, 3
Machado, M. E., Orwig, L. E., & Antonucci, E. 1986, Adv. Space Res., 6, 101
Mariska, J. T., Boris, J. P., Oran, E. S., Young, T. R., Jr., & Doschek, G. A. 1982, ApJ, 255, 738
Mariska, J. T., Emslie, A. G., & Li, P. 1989, ApJ, 341, 1067
McTiernan, J. M., Fisher, G. H., & Li, P. 1999, ApJ, 514, 472
Neupert, W. M. 1986, ApJ, 153, L59
Schmahl, E. J., et al. 1989, in Astrophysics and Space Science Library, Vol. 153, Energetic Phenomena on the Sun, ed. M. R. Kundu, B. Woodgate, & E. J. Schmahl (Dordrecht: Kluwer), chapter 1.4
Stoiser, S., Brown, J. C., & Veronig, A. M. 2008, Sol. Phys., 250, 315
Veronig, A., Vrsnak, B., Temmer, M., & Hanslmeier, A. 2002, Sol. Phys., 208, 297
Warren, H. P. 2006, ApJ, 637, 522